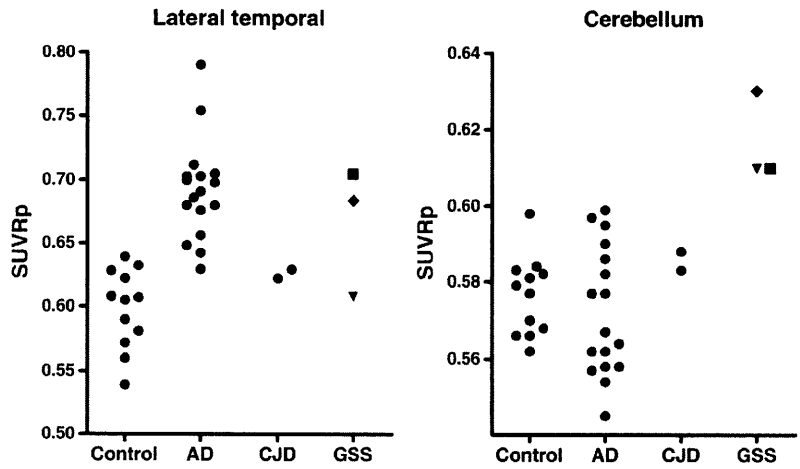

Fig. 4 SUVRp distribution in aged normal controls (*Control*), AD patients (*AD*), CJD patients (*CJD*) and GSS patients (*GSS*). GSS patients showed higher SUVRp values in the lateral temporal cortex and cerebellum. *Filled square* GSS1, *filled diamond* GSS2, *filled inverted triangle* GSS3

Discussion

This is the first study to demonstrate non-invasive detection of PrP amyloid plaques in GSS patients. GSS is neuropathologically characterized by deposits of multicentric amyloid plaques, which are especially abundant in the cerebellum, cerebral cortex and basal ganglia [3]. The present study demonstrated binding of BF-227 to PrP amyloid plaques in GSS brain sections. [^{11}C]BF-227 retention was observed in cortical and subcortical brain regions of GSS patients known for the high density of PrP plaques. Based on these findings, [^{11}C]BF-227 represents a promising candidate PET probe for the non-invasive detection of PrP amyloid plaques in the brain. However, the possibility that neocortical elevation of SUVRp in GSS patients might be caused by concomitant Aβ amyloid deposits or other misfolded protein deposits also should be considered, given that the two GSS patients showing prominent neocortical retention of [^{11}C]BF-227 were relatively older than the GSS patient showing no neocortical retention of BF-227. Although one positive GSS patient (GSS2) is still alive and was not examined neuropathologically, another positive case (GSS1) showed a high level of PrP amyloid deposits but no obvious deposits of Aβ amyloid or other misfolded proteins at autopsy. Furthermore, significant elevation of SUVRp was detected in the cerebellum, thalamus and hippocampus of all GSS cases. These brain regions are known to contain lower densities of Aβ plaques or other misfolded protein structures such as Lewy bodies. Based on these findings, it seems unlikely that concomitant deposition of Aβ amyloid or other misfolded proteins contributes to the high [^{11}C]BF-227 retention in GSS patients.

There is an increasing demand for in vivo detection of abnormal PrP deposition in the brain for the diagnosis of TSEs that might translate in early therapeutic intervention. Although GSS and other familial forms of TSEs can be diagnosed with PrP gene analysis using peripheral blood cells, it has been impossible to non-invasively measure the amount of abnormal PrP deposition in the brain. In a fashion similar to GSS, PrP amyloid deposition in the brain is commonly present in vCJD in which PrP amyloid plaques, called florid plaques, are pathognomonic [27]. Thus, [^{11}C]BF-227 PET might be a sensitive probe for the detection of PrP amyloid plaque deposition in vCJD as well as GSS, allowing longitudinal monitoring of PrP amyloid plaque deposition in the brain. Ante-mortem diagnosis of vCJD relies on the detection of abnormal PrP deposition in tonsil biopsy samples [28]. However, functional imaging using PET has an advantage over surgical biopsy tests in terms of both a non-invasive and an infection risk management point of view.

GSS is a rare form of TSE occurring in only about 3% of TSE cases in Japan. However, GSS is probably one of the TSEs most likely to benefit from early therapeutic interventions because the disease can be confirmed earlier using PrP gene analysis and progression occurs much more slowly than that in sporadic CJD, which comprises the majority of TSE cases. Recently, compounds such as pentosan polysulphate and doxycycline have been clinically used for experimental treatments for TSEs to prevent deposition of abnormal PrP in the brain, because these compounds slowed the disease progression in animal disease models when administered in an earlier stage of the disease [29–33]. Reliable surrogate markers are also required to evaluate the efficacy of these experimental interventions, and [^{11}C]BF-227 PET might be one of the best candidates to assess PrP amyloid deposition in GSS. However, it remains to be elucidated if PrP amyloid levels are a particularly relevant marker of therapeutic efficacy.

A previous PET study demonstrated moderate FDDNP retention and no remarkable PIB retention in the brain of two familial CJD patients with an octapeptide repeat insertion mutation [17]. A recent PET study has additionally demonstrated no PIB retention in two autopsy-confirmed sporadic

CJD patients [18]. In contrast with these studies, the present study successfully demonstrated prominent [^{11}C]BF-227 retention in the brain of GSS patients. Differences between the previous and present findings might mainly reside in the amount and type of PrP amyloid deposits in the brain, where histopathological studies indicate higher density of PrP amyloid plaques in GSS than in familial CJD [1]. In the present study, the findings in two sporadic CJD patients showing no obvious [^{11}C]BF-227 retention in the brain additionally support this speculation. The difference may also be attributable to higher binding affinity of BF-227 to PrP amyloid cores compared to FDDNP and PIB. To clarify this, further in vitro studies comparing the binding affinities of different amyloid tracers to PrP plaques in TSE brain homogenates are needed.

The youngest GSS patient (GSS3) showed BF-227 retention in the cerebellum and thalamus but not in the neocortex. The clinical symptoms in this patient were consistent with the brain distribution of BF-227, with the patient presenting with severe gait disturbance and slurred speech resulting from cerebellar ataxia but no signs of cognitive impairment, suggesting a close relationship between PrP plaque deposition as measured by BF-227 and regional brain dysfunction. There are variations of clinical phenotypes in GSS [1, 3]. Such variations are yet to be explained; however, the pattern of regional PrP amyloid distribution might be one of the factors affecting clinical phenotypes of GSS. In vivo PrP amyloid imaging using [^{11}C]BF-227 or other PET tracers will clarify neuropathological aspects of clinical variations in GSS.

In summary, we confirmed binding of BF-227 to PrP plaques in vitro and in vivo. A clinical PET study using [^{11}C]BF-227 demonstrated in vivo detection of PrP amyloid plaques in GSS patients. This imaging technique provides a potential means of facilitating both early diagnosis and non-invasive disease monitoring of certain forms of TSEs because, despite a lack of selectivity for PrP, brain retention of BF-227 in GSS shows a distinct pattern of regional distribution than that usually observed in sporadic AD.

Acknowledgment We appreciate the assistance of Dr. S. Watanuki, Dr. M. Miyake and Dr. H. Takashima in the clinical PET studies. This study was supported in part by the Program for the Promotion of Fundamental Studies in Health Science of the NIBIO in Japan, Industrial Technology Research Grant Program of the NEDO in Japan, and Health and Labor Sciences Research Grants (Translational Research and Research on Measures for Intractable Diseases) from the Ministry of Health, Labor, and Welfare of Japan.

References

1. DeArmond SJ, Kretzschmar HA, Prusiner SB. Prion diseases. In: Graham DI, Lantos PL, editors. Greenfield's neuropathology, 7th ed. London: Hodder Arnold. p. 273–323.
2. Collins SJ, Lawson VA, Masters CL. Transmissible spongiform encephalopathies. Lancet 2004;363:51–61.
3. Collins S, McLean CA, Masters CL. Gerstmann-Sträussler-Scheinker syndrome, fatal familial insomnia, and kuru: a review of these less common human transmissible spongiform encephalopathies. J Clin Neurosci 2001;8:387–97.
4. Noguchi-Shinohara M, Hamaguchi T, Kitamoto T, Sato T, Nakamura Y, Mizusawa H, et al. Clinical features and diagnosis of dura mater graft associated Creutzfeldt Jakob disease. Neurology 2007;69:360–7.
5. Lasmézas CI, Deslys JP, Demaimay R, Adjou KT, Hauw JJ, Dormont D. Strain specific and common pathogenic events in murine models of scrapie and bovine spongiform encephalopathy. J Gen Virol 1996;77(Pt 7):1601–9.
6. Schulz-Schaeffer WJ, Tschöke S, Kranefuss N, Dröse W, Hause-Reitner D, Giese A, et al. The paraffin-embedded tissue blot detects PrP(Sc) early in the incubation time in prion diseases. Am J Pathol 2000;156:51–6.
7. Fraser JR. What is the basis of transmissible spongiform encephalopathy induced neurodegeneration and can it be repaired? Neuropathol Appl Neurobiol 2002;28:1–11.
8. Small GW, Kepe V, Ercoli LM, Siddarth P, Bookheimer SY, Miller KJ, et al. PET of brain amyloid and tau in mild cognitive impairment. N Engl J Med 2006;355:2652–63.
9. Klunk WE, Engler H, Nordberg A, Wang Y, Blomqvist G, Holt DP, et al. Imaging brain amyloid in Alzheimer's disease with Pittsburgh Compound-B. Ann Neurol 2004;55:306–19.
10. Verhoeff NP, Wilson AA, Takeshita S, Trop L, Hussey D, Singh K, et al. In-vivo imaging of Alzheimer disease beta-amyloid with [11C]SB-13 PET. Am J Geriatr Psychiatry 2004;12:584–95.
11. Rowe CC, Ackerman U, Browne W, Mulligan R, Pike KL, O'Keefe G, et al. Imaging of amyloid beta in Alzheimer's disease with 18F-BAY94–9172, a novel PET tracer: proof of mechanism. Lancet Neurol 2008;7:129–35.
12. Kudo Y, Okamura N, Furumoto S, Tashiro M, Furukawa K, Maruyama M, et al. 2-(2-[2-Dimethylaminothiazol-5-yl]ethenyl)-6-(2-[fluoro]ethoxy)benzoxazole: a novel PET agent for in vivo detection of dense amyloid plaques in Alzheimer's disease patients. J Nucl Med 2007;48:553–61.
13. Ishikawa K, Doh-ura K, Kudo Y, Nishida N, Murakami-Kubo I, Ando Y, et al. Amyloid imaging probes are useful for detection of prion plaques and treatment of transmissible spongiform encephalopathies. J Gen Virol 2004;85:1785–90.
14. Bresjanac M, Smid LM, Vovko TD, Petric A, Barrio JR, Popovic M. Molecular-imaging probe 2-(1-[6-[(2-fluoroethyl)(methyl) amino]-2-naphthyl]ethylidene) malononitrile labels prion plaques in vitro. J Neurosci 2003;23:8029–33.
15. Sadowski M, Pankiewicz J, Scholtzova H, Tsai J, Li Y, Carp RI, et al. Targeting prion amyloid deposits in vivo. J Neuropathol Exp Neurol 2004;63:775–84.
16. Hoefert VB, Aiken JM, McKenzie D, Johnson CJ. Labeling of the scrapie-associated prion protein in vitro and in vivo. Neurosci Lett 2004;371:176–80.
17. Boxer AL, Rabinovici GD, Kepe V, Goldman J, Furst AJ, Huang SC, et al. Amyloid imaging in distinguishing atypical prion disease from Alzheimer disease. Neurology 2007;69:283–90.
18. Villemagne VL, McLean CA, Reardon K, Boyd A, Lewis V, Klug G, et al. 11C-PiB PET studies in typical sporadic Creutzfeldt-Jakob disease. J Neurol Neurosurg Psychiatry 2009;80:998–1001. doi:10.1136/jnnp.2008.171496.
19. Okamura N, Suemoto T, Shimadzu H, Suzuki M, Shiomitsu T, Akatsu H, et al. Styrylbenzoxazole derivatives for in vivo imaging of amyloid plaques in the brain. J Neurosci 2004;24:2535–41.
20. Ishikawa K, Kudo Y, Nishida N, Suemoto T, Sawada T, Iwaki T, et al. Styrylbenzoazole derivatives for imaging of prion plaques and treatment of transmissible spongiform encephalopathies. J Neurochem 2006;99:198–205.

21. Waragai M, Okamura N, Furukawa K, Tashiro M, Furumoto S, Funaki Y, et al. Comparison study of amyloid PET and voxel-based morphometry analysis in mild cognitive impairment and Alzheimer's disease. J Neurol Sci 2009;285:100–8. doi:10.1016/j.jns.2009.06.005.
22. Okamura N, Furumoto S, Funaki Y, Suemoto T, Kato M, Ishikawa Y, et al. Binding and safety profile of novel benzoxazole derivative for in vivo imaging of amyloid deposits in Alzheimer's disease. Geriatr Gerontol Int 2007;7:393–400.
23. Zeidler M, Gibbs CJ Jr, Meslin F. WHO manual for strengthening diagnosis and surveillance of Creutzfeldt-Jakob disease. Geneva: World Health Organization; 1998. p. 47–51.
24. McKhann G, Drachman D, Folstein M, Katzman R, Price D, Stadlan EM. Clinical diagnosis of Alzheimer's disease: report of the NINCDS-ADRDA Work Group under the auspices of Department of Health and Human Services Task Force on Alzheimer's Disease. Neurology 1984;34:939–44.
25. Friston KJ, Holmes AP, Worsley KJ, Poline JP, Frith CD, Frackowiack RSJ. Statistical parametric maps in functional imaging: a general linear approach. Hum Brain Mapp 1995;2:189–210.
26. Masters CL, Gajdusek DC, Gibbs CJ Jr. Creutzfeldt-Jakob disease virus isolations from the Gerstmann-Sträussler syndrome with an analysis of the various forms of amyloid plaque deposition in the virus-induced spongiform encephalopathies. Brain 1981;104:559–88.
27. Ironside JW, McCardle L, Horsburgh A, Lim Z, Head MW. Pathological diagnosis of variant Creutzfeldt-Jakob disease. APMIS 2002;110:79–87.
28. Hill AF, Zeidler M, Ironside J, Collinge J. Diagnosis of new variant Creutzfeldt-Jakob disease by tonsil biopsy. Lancet 1997;349:99–100.
29. Doh-ura K, Ishikawa K, Murakami-Kubo I, Sasaki K, Mohri S, Race R, et al. Treatment of transmissible spongiform encephalopathy by intraventricular drug infusion in animal models. J Virol 2004;78:4999–5006.
30. Rainov NG, Tsuboi Y, Krolak-Salmon P, Vighetto A, Doh-Ura K. Experimental treatments for human transmissible spongiform encephalopathies: is there a role for pentosan polysulfate? Expert Opin Biol Ther 2007;7:713–26.
31. De Luigi A, Colombo L, Diomede L, Capobianco R, Mangieri M, Miccolo C, et al. The efficacy of tetracyclines in peripheral and intracerebral prion infection. PLoS One 2008;3:e1888.
32. Teruya K, Kawagoe K, Kimura T, Chen CJ, Sakasegawa Y, Doh-ura K. Amyloidophilic compounds for prion diseases. Infect Disord Drug Targets 2009;9:15–22.
33. Forloni G, Salmona M, Marcon G, Tagliavini F. Tetracyclines and prion infectivity. Infect Disord Drug Targets 2009;9:23–30.

Original Paper

Fetal Diagnosis and Therapy

Fetal Diagn Ther 2010;28:79–86
DOI: 10.1159/000316102

Received: October 12, 2009
Accepted after revision: May 25, 2010
Published online: July 31, 2010

Effects of Antenatal Steroid Therapy on Neurodevelopment in an IUGR Mouse Model

Clarissa Velayo[a] Takuya Ito[b] Hiroshi Chisaka[a] Nobuo Yaegashi[a]
Kunihiro Okamura[a] Yoshitaka Kimura[a, b]

[a]Department of Obstetrics and Gynecology, Tohoku University Graduate School of Medicine, and
[b]International Advanced Research and Education Organization, Tohoku University, Sendai, Japan

Key Words
Antenatal steroid therapy · Dexamethasone · Intrauterine growth restriction mouse model · Maternal protein restriction, mice · Postnatal neurodevelopment

Abstract
Background/Objective: To investigate the neurodevelopmental response in postnatal mice secondary to antenatal steroid treatment in association with maternal protein restriction. ***Methods:*** C57BL/6N pregnant mice (n = 24; 4 per treatment group) were administered control (C) or protein-restricted (PR) diets and subjected to daily subcutaneous injection stress during late gestation (E10–E17) with either 100 μl/kg of dexamethasone sodium phosphate in normosaline (C-D/S, PR-D/S) or normosaline alone (C-S, PR-S). Non-treatment groups were also included (C, PR). Brain samples of pups were collected on postnatal day 7 and analyzed by immunohistochemistry and qRT-PCR. ***Results:*** Neonatal weights in the treatment groups were smaller than their counterparts in the C group, but there were no significant differences in brain size. Immunohistochemical evaluation of neuroglial cells revealed a pronounced effect of protein restriction on oligodendrocytes and oligodendrocyte precursor cells with distinct fetal responses to stress and dexamethasone. Further evaluation using quantitative RNA analysis showed significant activation of *Galr1*, *Galr2*, *Igfbp-1*, *Igfbp-3*, *Igfbp-6*, and *Fgf2* by 1- to 2.5-fold in the PR-D/S group and by much higher increments, 1- to 10.5-fold, in the PR-S group. ***Conclusion:*** This preliminary investigation revealed the possible role of dexamethasone in further increasing vulnerability to cell damage in injury-prone neuroglial cells. The distribution of key glial markers and the overexpression of several neurotrophic factors depicted ongoing cellular adaptation.

Introduction

At the present time, antenatal steroid therapy is an option for which the benefits seem to outweigh the risks, but this generalization may not apply to all patients. There are two types of preterm infants according to birth weight: (1) preterm infants with appropriate weight for gestational age, and (2) preterm infants with low birth weight for gestational age. The latter group is known to be more susceptible to chronic diseases and diseases of adult onset [1]. This vulnerability may be attributed to adaptive responses during development secondary to environmental stimuli such as maternal diet modification and stress which instigate changes in fetal programming.

KARGER
Fax +41 61 306 12 34
E-Mail karger@karger.ch
www.karger.com

1015–3837/10/0282–0079$26.00/0

Accessible online at:
www.karger.com/fdt

Clarissa Velayo, MD
Department of Obstetrics and Gynecology
Tohoku University Graduate School of Medicine
1-1, Seiryomachi, Aoba-ku, Sendai 980-8574 (Japan)
Tel. +81 22 717 7251, Fax +81 22 717 7258, E-Mail chinkeyvelayo@yahoo.com

In this study, a novel approach to understanding fetal adaptive response as graded events is presented. All structural levels may be observed to follow a temporal pattern of events wherein acute and chronic responses depend on surpassing specific thresholds. A primary exposure that does not surpass the threshold for an adaptive response results in sensitization with minimal changes to the developing fetus. On the other hand, single or cumulative exposures that surpass the threshold can mount an adaptive response. Furthermore, graded events before and after the attainment of such thresholds have also been observed in this study. A hyperreactive response, occurring in pre-sensitized fetuses, will exhibit lower thresholds while a restrained response is a subdued or muted change observed in pre-sensitized fetuses in the presence of dexamethasone.

This study uses protein restriction in a mouse model for simulation of intrauterine growth restriction (IUGR) and focuses on the effects of antenatal steroid therapy on postnatal neurodevelopment. The neuroplasticity of glial cells allows for the observation of such changes. Through the use of stage-specific markers, different glial populations can be delineated during embryonic brain development [2–4]. For our study purposes, two types of glial cells were evaluated: oligodendrocytes *(Mbp* and *Pdgfrα)* and astrocytes *(Gfap)* – both of which are derived from a common precursor *(Olig2).*

In addition, specific gene expression was evaluated to characterize ongoing cellular adaptation. Numerous investigations concerning the different oligodendrocyte lineage cells have reported that these genes are regulators of growth *(Igfbp-1, Igfbp-3,* and *Igfbp-6)* and have neuroprotective properties *(Galr1, Galr2,* and *Fgf2)* among which include the prevention of demyelination and the enhancement of neurogenesis after injury [5–13].

Thus, neonatal brain phenotypic attributes neuroglial protein patterns and mRNA expression of neurotrophic genes were evaluated for their response to dexamethasone treatment.

Materials and Methods

Animals

Female C57BL/6N mice (n = 24), about 6 weeks old, provided by the Institute for Animal Experimentation, Tohoku University Graduate School of Medicine, were maintained under controlled lighting (12-hour light cycles) and temperature (24°C). These were allowed free access to food (AIN-93G; Oriental Yeast Co. Ltd, Tokyo, Japan) and water during a 2-week acclimatization period after which each female was time mated with a male.

Treatment Groups

Pregnant females were housed singly and administered either control (C) or protein-restricted (PR) diets (online suppl. table 1, www.karger.com/doi/10.1159/000316102) ad libitum all throughout pregnancy (embryonic stage, E0–E17) and after delivery (postnatal stage, P0–P7). These were further subdivided into six groups (n = 4 per group) where each received a single or combination of treatments during late gestation (E10–E17). More specifically, this consisted of daily subcutaneous injection stress with either plain normosaline solution (C-S, PR-S) or 100 μl/kg dexamethasone sodium phosphate (Decadron®; MSD Banyu Pharmaceutical Co. Ltd, Japan) in normosaline solution (C-D/S, PR-D/S). Non-treatment groups were also included (C, PR). All injections were performed between 12 and 2 p.m. Maternal weights on days E0, E10, and E17 were recorded, as well as neonatal weights on P7.

Whole Brain Sampling

On postnatal day 7, separate brain sampling techniques were performed. For brain size and immunohistochemical analyses (n = 96; 16 per treatment), 2 male and 2 female pups from each litter were anesthetized by isoflurane inhalation (Forane® Isoflurane; Abbott Japan Co. Ltd, Japan) and perfused intracardially with 4% paraformaldehyde. Whole brains were collected and supercooled in dry ice for 30 min before storage at –20°C. These were subsequently mounted using an OCT compound (Tissue-Tek® 4583; Sakura Finetek Japan, Co. Ltd, Tokyo, Japan) and cut on a cryostat (Leica Cryostat CM3050 S; Leica, Wetzlar, Germany) to obtain 14-μm coronal sections at the level of the lateral ventricle (bregma = 0–0.74 mm, interaural = 3.80–4.39 mm). All specimens were collected on APS-coated Superfrost glass microslides (Matsunami Glass Ind. Ltd, Osaka, Japan) and air dried. Sections were stored at –80°C. Meanwhile for RNA analysis, whole brain samples from the remaining pups in each litter (n = 42; 7 per treatment) underwent initial processing for later RNA extraction. The same anesthetic procedure mentioned earlier was applied prior to brain dissection followed by supercooling in liquid nitrogen and storage at –80°C.

Fetal Brain Size Analysis

Slide sections were stained with hematoxylin (Gill's Hematoxylin 2003-2; Muto Pure Chemicals Co. Ltd., Japan) and eosin (Eosin Alcohol Solution acid extract 050-06041; Wako Pure Chemicals, Ind. Ltd, Japan). Images were captured on a Leica CTR 5000 and DM 5000B microscope system (Leica). Using Adobe® Photoshop® CS4 Extended software, specific brain portions were manually traced on each of the captured digital images and the total number of pixels within traced areas was determined. Individual cortical thicknesses as well as corpus callosum indices were analyzed. The latter was equal to the ratio of the area of the corpus callosum and the cortical thickness.

Immunohistochemistry

A total of 16 fetal brains (8 male, 8 female) per treatment group were examined. Sections were blocked with 4% paraformaldehyde for 15 min and incubated with the primary antibody at 4°C overnight. Coupled secondary antibodies were used for single and double labeling. Slides were mounted with Vectashield® medium (Vector Laboratories, Inc., Burlingame, Calif., USA) and coverslipped. The following primary antibodies were used: Mbp (Rat

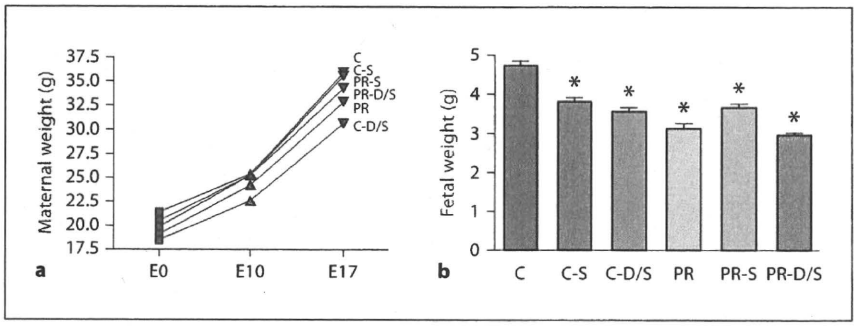

Fig. 1. Effects of treatment on weight gain. **a** Each data point represents maternal weight as mean ± SD (n = 4 per treatment). Two-way ANOVA indicates a significant treatment effect ($p < 0.0001$) and time effect ($p < 0.0001$). Bonferroni post-test indicates that, with the exception of the PR and C-D/S groups at E17, all treatments were similar to the C group. **b** Mean fetal weights across treatments ± SEM were significantly different by one-way ANOVA ($p < 0.0001$; n = 193). Bonferroni post-test indicates significant variation of the C group with all other treatment groups (* $p < 0.001$).

Anti-Myelin basic protein 82–87 region IgG; 1:200; Chemicon International, Inc., Temecula, Calif., USA), Gfap (Rabbit anti-glial fibrillary acidic protein IgG; 1:800; Sigma, St. Louis, Mo., USA), Olig2 (Anti-Human Olig2 Rabbit IgG Affinity Purity; 1:1,000; IBL, Co. Ltd, Japan), and Pdgfrα (Purified rat anti-mouse CD140a (PDGF Receptor α chain monoclonal antibody IgG; 1:500; BD Pharmingen, San Diego, Calif., USA). 4′6-Diamidino-2-phenylindole, dihydrochloride (DAPI) FluoroPure™ grade (1:500; Molecular Probes, Inc., Eugene, Oreg., USA) was used to identify the nuclei. The following secondary antibodies were used: Alexa Fluor® 488 donkey anti-rabbit IgG (1:500; Invitrogen, Eugene, Oreg., USA) and Cy™3-conjugated Affini-Pure Donkey anti-rat IgG (1:500; Jackson ImmunoResearch Laboratories, Inc., West Grove, Pa., USA). Images were captured on a Leica CTR 5000 and DM 5000B microscope system (Leica). Neuroglial protein marker expression was analyzed using Adobe Photoshop® CS4 Extended software. Specific brain portions were manually traced on each of the captured digital images. Protein marker expression was equivalent to the degree of fluorescence observed (pixels of fluorescence/total number of pixels) (online suppl. fig. 1).

Quantitative PCR

Total RNA was extracted from whole fetal brains using QIAzol Lysis Reagent (Qiagen, Hilden, Germany) and cleaned with an miRNeasy kit (Qiagen) according to the manufacturer's protocol. Complementary DNA was synthesized using the Superscript™III First-Strand Synthesis System (Invitrogen, Carlsbad, Calif., USA) and quantitative PCR was conducted with Express SYBR® GreenER™ Supermix with Premixed ROX (Invitrogen) on an Eppendorf *Realplex²* Mastercycler (Eppendorf, Hamburg, Germany). Primer sequences of the resulting significant genes are provided (online suppl. table 2).

Statistical Analysis

One-way analysis of variance (ANOVA) was conducted between treatment groups for each procedure. Post-hoc analysis (Bonferroni post-test) was also used where applicable. All tests were performed using GraphPad Prism® 4 software.

Results

Maternal weight gain patterns between groups were similar before (E0–E10) and during treatment (E10–E17). There were no differences in timing of delivery (E18 or P0), litter size, and litter sex distribution. Mean neonatal weights on postnatal day 7 between treatment groups were significantly different ($p < 0.0001$; n = 193) showing a mean decrease of all groups compared to the C group (fig. 1). However, fetal brain size across treatment groups were similar (n = 91). The cortical thickness between treatment groups did not differ and corpus callosum indices revealed proportionality of this area to cortical thickness independent of the treatment received (fig. 2).

Immunohistochemical Analysis

The immunohistochemical analysis of *Mbp* and *Gfap* expression, mature oligodendrocyte and astrocyte markers, respectively, demonstrated that astrocyte populations were less affected by protein restriction or injection stress. However, like oligodendrocyte populations, these were not resilient against dexamethasone (fig. 3).

Diet-affected patterns across treatment groups in the corpus callosum *(cc)* were notably similar between *Mbp* and *Pdgfrα* (fig. 3, 4) revealing a more pronounced effect on oligodendrocytes. For *Pdgfrα* and *Olig2*, the additional analysis of adjacent brain areas such as the subventricular zone *(svz)* (fig. 4c, f) and caudate putamen *(cpu)* (fig. 4d, g) exhibited the same expression patterns producing no geographical distinction.

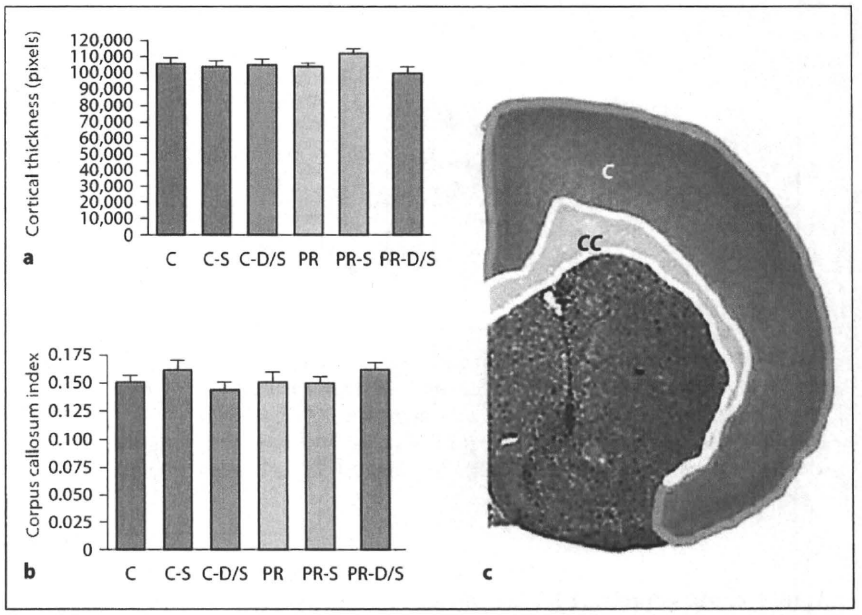

Fig. 2. a, b Cortical thickness and corpus callosum indices suggested similarity between fetal brain size across treatments with standard error bars included (n = 91). **c** The corpus callosum index was equal to the ratio of the area of the corpus callosum *cc* and the cortical thickness *c*.

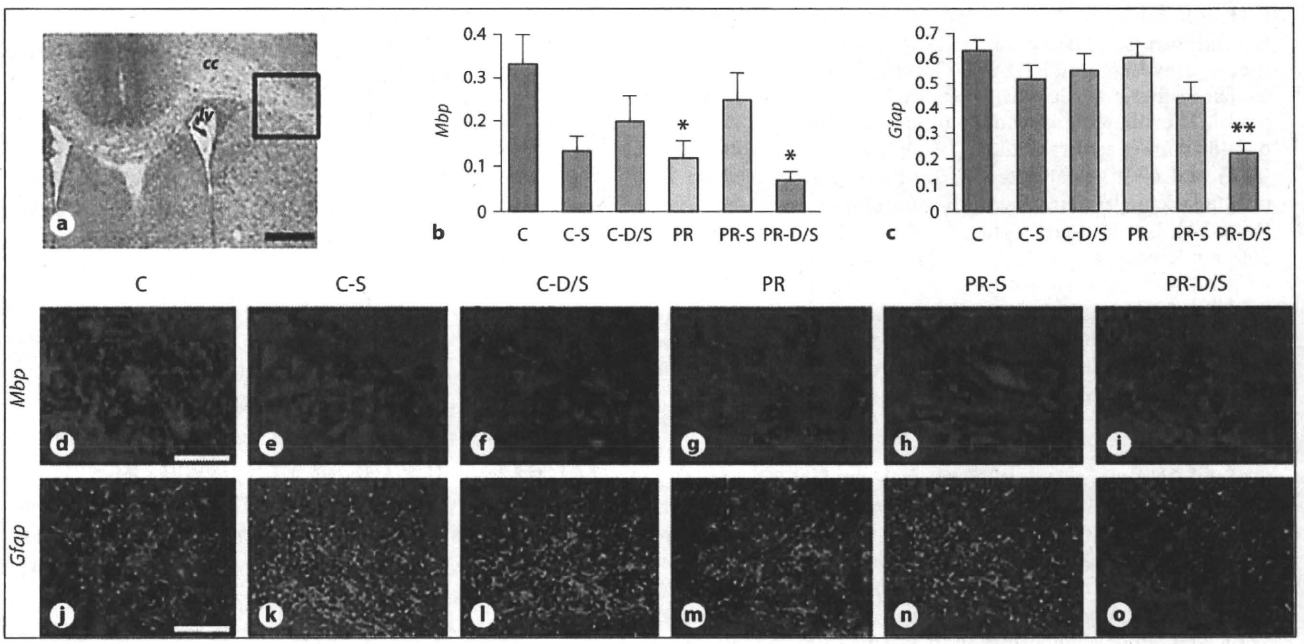

Fig. 3. Mbp and Gfap expression in the six treatment groups. **a** Box inset shows the approximate area measured in the corpus callosum *cc* in a coronal section at the level of the lateral ventricle *lv* using hematoxylin and eosin staining. **b, c** Graphical representations summarizing immunohistochemical results as ratio of positive area by *cc* area for each marker (standard error bars included). One-way ANOVA indicates significant variation in both *Mbp* ($p < 0.0027$; n = 85) and *Gfap* ($p < 0.0001$; n = 86). A comparison to the C group by Bonferroni post-test shows significant variation with the PR (* $p < 0.05$) and PR-D/S (* $p < 0.01$; ** $p < 0.001$) groups. **d–o** Representative images for each treatment group showing *Mbp* (**d–i**) and *Gfap* (**j–o**) expression at a magnification of 20×. Scale bars: **a** = 500 μm, **d–o** = 200 μm.

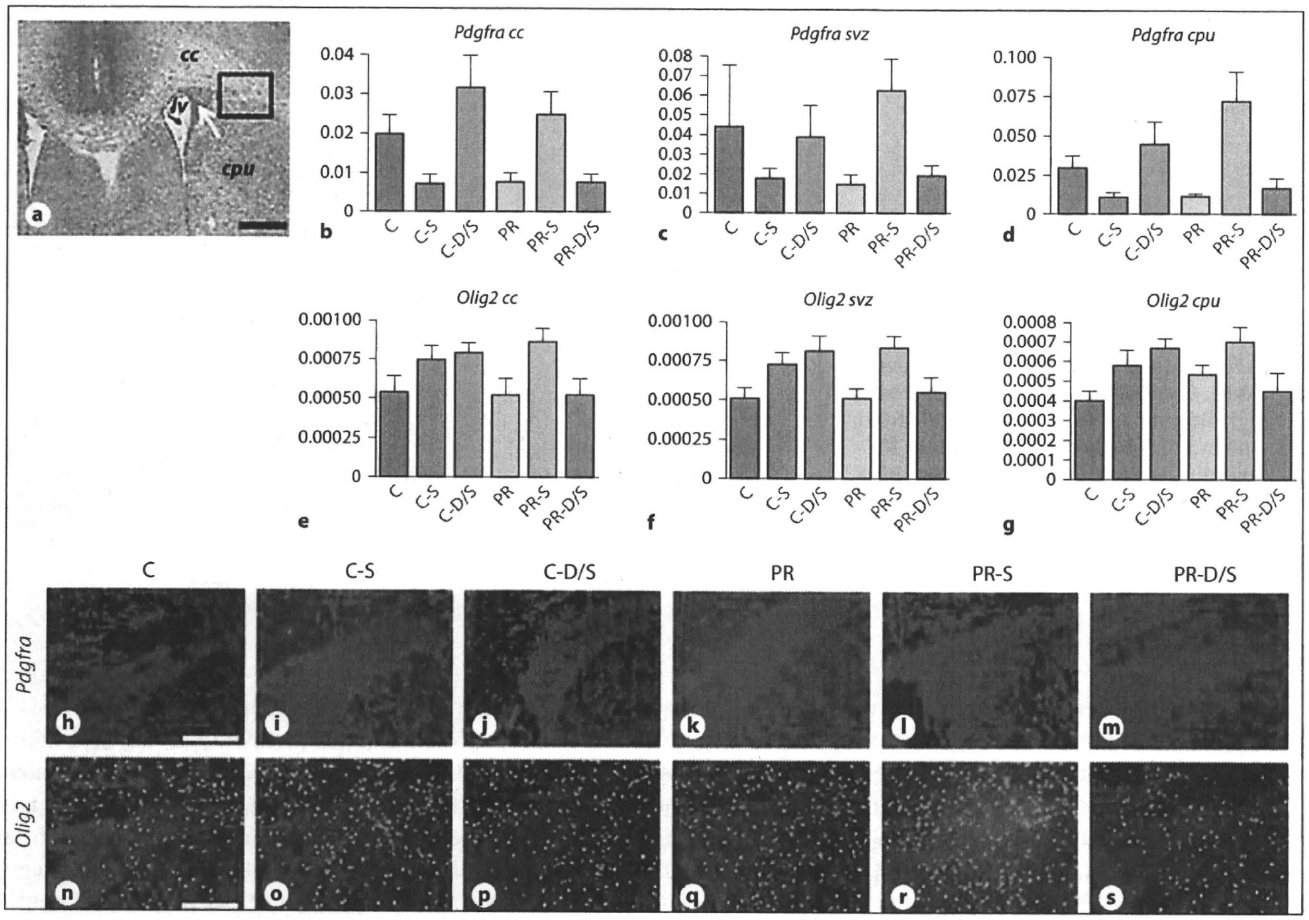

Fig. 4. *Pdgfra* and *Olig2* expression in the six treatment groups. **a** Box inset shows the approximate area measured in a coronal section at the level of the lateral ventricle *(lv)* using HE staining; corpus callosum *(cc)*; caudate putamen *(cpu)*; white arrow, subventricular zone *(svc)*. **b–g** Graphical representations summarizing immunohistochemical results as ratio of positive area by specified brain area for each marker (standard error bars included). Statistical analyses were significant using one-way ANOVA for *Pdgfra cc* ($p < 0.0002$; $n = 85$), *Pdgfra cpu* ($p < 0.0001$; $n = 85$), *Olig2 cc* ($p < 0.0240$; $n = 83$), *Olig2 svz* ($p < 0.0044$; $n = 83$), and *Olig2 cpu* ($p < 0.0166$; $n = 83$). **h–s** Representative images for each treatment group showing *Pdgfra* (**h–m**) and *Olig2* (**n–s**) expression at a magnification of 20×. Scale bars: **a** = 500 μm, **h–s** = 200 μm.

mRNA Analysis

Quantitative RNA analysis showed significant activation ($p < 0.0001$) of *Galr1*, *Galr2*, *Igfbp-1*, *Igfbp-3*, *Igfbp-6*, and *Fgf2* by 1- to 2.5-fold in the PR-D/S group and by much higher increments, 1- to 10.5-fold, in the PR-S group (fig. 5).

Discussion

The expression patterns across treatment groups were indicative of varying responses to injury in both oligodendrocyte and astrocyte lineage cells. First, there were different effects between neuroglial cell types secondary to primary injury. Second, the effect of protein restriction on oligodendrocyte distribution patterns was more pronounced, but the specific precursor cell lineage most affected was not determined, and third, significant genes pointed towards oligodendrocyte susceptibility and myelination effects. From these, a key response to dexamethasone was seen as a recurring pattern in the PR-S and PR-D/S groups in both immunohistochemical evaluation and mRNA analysis (fig. 3–5).

Maintaining glucocorticoid homeostasis necessitates a delicate balance between maternal and fetal environments. Our results suggested that mice in the C diet treat-

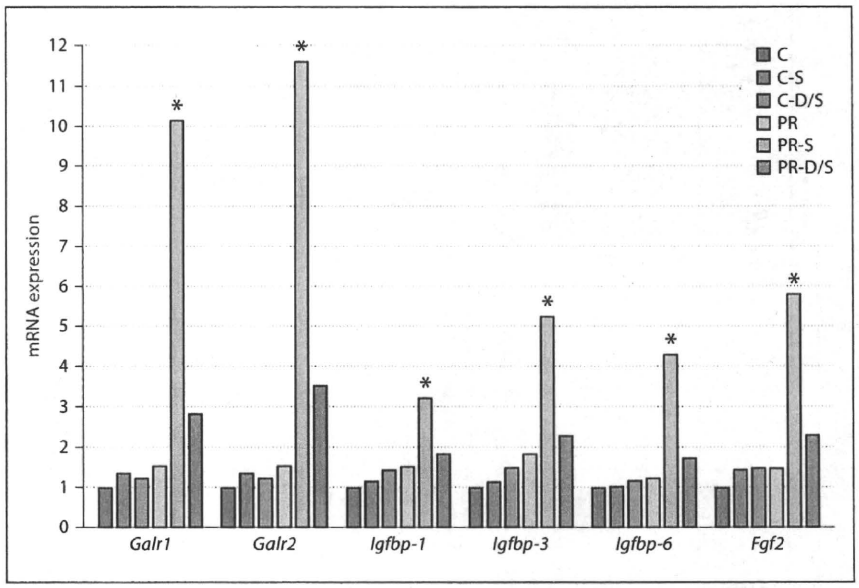

Fig. 5. Quantitative mRNA analysis. There was significant activation by one-way ANOVA ($p < 0.0001$; $n = 24$ per gene) of *Galr1, Galr2, Igfbp-1, Igfbp-3, Igfbp-6,* and *Fgf2* by 1- to 2.5-fold in the PR-D/S group and by much higher increments, 1- to 10.5-fold, in the PR-S group. Bonferroni post-test indicated * $p < 0.001$ for PR-S. Individual gene graphs with standard error reports were submitted as online supplementary figure 1.

ment groups were able to maintain varying levels of glucocorticoid homeostasis amidst chronic stress (daily subcutaneous injections from E10 to E17) or the presence of dexamethasone. In C group offspring, exposure to normal levels of maternal cortisol was successfully blocked. In C-S offspring, increased levels of maternal endogenous cortisol overwhelmed this natural protective barrier and led to significant fetal exposure. Both exogenous and eventually endogenous corticosteroids resulted in IUGR effects at phenotypic and molecular levels. C-S fetuses were sensitized or became susceptible to any further change. In the C-D/S offspring, IUGR was evident, but the addition of dexamethasone resulted in an adaptive fetal response not observed with stress alone. In terms of neurodevelopmental effects, our results showed that this was a beneficial or protective response to stress.

On the other hand, mice in the PR diet groups were basically at a disadvantage prior to stress or dexamethasone treatment. The offspring of PR groups were pre-sensitized. Aside from exhibiting IUGR, they most likely had dysfunctional placentas. With the addition of chronic stress (PR-S), a protective hyperreactive fetal response was observed, but this response was markedly restrained in the presence of dexamethasone (PR-D/S). The latter suggested detrimental effects to neurodevelopment in the last treatment group.

The presence of a protective barrier system between this interplay of maternal and fetal environments is crucial. Current investigations have focused on the role of 11β-hydroxysteroid dehydrogenase type 2 (11-βHSD2) as a possible placental glucocorticoid barrier, and interestingly, 11-βHSD2 activity is decreased during maternal protein restriction or stress [14]. This would explain how high maternal cortisol concentrations were able to saturate the limited enzyme available allowing any excess to pass through unchanged. This presents distinct similarities with our study conditions, but the presence of 11-βHSD2 alone cannot account for the graded fetal response observed or the isolated effects of dexamethasone.

Dexamethasone was administered subcutaneously thereby effectively bypassing maternal liver metabolism. It was also less difficult for this glucocorticoid to reach the fetus because it has been known to be a poor substrate for placental 11-βHSD2 [15]. Two possible explanations for the observed isolated dexamethasone effects in contrast to cortisol were as follows: first, the supraphysiological levels and potency of dexamethasone may have produced these damaging effects. Dexamethasone was notably the more potent glucocorticoid with a potency range of 25–80 and $t_{1/2}$ (half-life in hours) of 36–54, as compared to cortisol with a potency of 1 and $t_{1/2}$ of 8 [16]. Second, due to anti-inflammatory properties which have not been fully elucidated yet, corticosteroids bind to receptors and form complexes that target genes in the nucleus [17]. It is possible that there was differential regulation of target genes between dexamethasone and cortisol, or due to individual properties, they differed entirely in terms of specific genes targeted. Furthermore, suppression of the

fetal HPA axis could not possibly account for all phenotypic results and underlying genotypic alterations. More likely, the effects of dexamethasone result from a collective response from various structural levels (molecular to cellular) both involving fetal neurometabolic factors and maternal adaptation to pregnancy.

Our IUGR mouse model developed at the Tohoku University has been modified for different investigative projects [18–22], but its main premise asserts that maternal malnutrition in mice affects offspring and acts as a primary insult or an acquired susceptibility resulting in phenotypic and genotypic changes. In addition, this study also recognized another primary insult as stress in the form of an injection. This implication is supported by various studies where injection of a vehicle alone was not equivalent to a placebo due to resulting behavioral and biochemical modulation [23, 24]. In the analysis of this study, understanding these two sources of primary insults and their roles in each treatment group helped to delineate which effects of those observed were truly attributable to dexamethasone alone. The treatment groups where only a primary injury was involved (C-S, PR) may or may not have shown marked differences from the C group, but their underlying sensitization to further injury can be inferred from the behavior of double injury treatments (C-D/S, PR-S).

Another concern was the brain area chosen in the experiment. Conventional reports focus on the hippocampus, but more investigations have started to look at other subcortical areas, such as the corpus callosum and subventricular zone, where there also exists high neuroplastic potential extending into the postnatal and adult period [4–6]. Moreover, oligodendrocyte lineage precursors have been demonstrated to migrate from different parts of the telencephalic ventricular zone towards various neural segments in waves beginning in the late gestation [4]. Thus, an examination of glial movement patterns should be included in future studies.

Dexamethasone: Good or Bad for the Brain?

In summary, prenatal programming, secondary to maternal protein restriction, renders an inherent susceptibility to neural compromise in offspring. This was evident in our study of two neuroglial cell lines. This early vulnerability or pre-sensitization uniquely changes fetal response to further injury as compared to other forms of stress. With the addition of dexamethasone in PR offspring, the restrained response may be seen as more detrimental than beneficial.

Clinical Correlation

Consensus dictates that the benefits should always outweigh the risks. In relation to antenatal steroid therapy, benefits related to organ maturation still mark heavily. Furthermore, the amount of dexamethasone administered to mice in this experiment were at supraphysiological levels and cannot be compared to current practice guidelines on antenatal steroid therapy, but our concern remains for incidences where multiple treatment is necessary in low-birth-weight or IUGR babies. It is for these extreme, but no less important, cases that more studies should attempt to understand beyond the general perception to achieve truly individualized medicine.

Acknowledgements

The authors would like to thank K. Mitsuya, N. Nakamura, J. Sharif, N. Matsuda, and M. Wong-Radescu for their assistance. Dr. Velayo is a Takeda Science Foundation Fellow.

References

1 Seckl JR, Holmes MC: Mechanisms of disease: glucocorticoids, their placental metabolism and fetal 'programming' of adult pathophysiology. Nat Clin Pract Endocrinol Metab 2007;3:479–488.

2 Liu Y, Wu Y, Lee JC, Xue H, Pevny LH, Kaprielian Z, et al: Oligodendrocyte and astrocyte development in rodents: an in situ and immunohistological analysis during embryonic development. Glia 2002;40:25–43.

3 Cai J, Chen Y, Cai WH, Hurlock EC, Wu H, Kernie SG, et al: A crucial role for Olig2 in white matter astrocyte development. Development 2007;134:1887–1899.

4 Kessaris N, Fogarty M, Iannarelli P, Grist M, Wegner M, Richardson WD: Competing waves of oligodendrocytes in the forebrain and postnatal elimination of an embryonic lineage. Nat Neurosci 2006;9:173–179.

5 Shen PJ, Larm JA, Gundlach AL: Expression and plasticity of galanin systems in cortical neurons, oligodendrocyte progenitors and proliferative zones in normal brain and after spreading depression. Eur J Neurosci 2003; 18:1362–1376.

6 Shen PJ, Yuan CG, Ma J, Cheng S, Yao M, Turnley AM, et al: Galanin in neuro(glio)-genesis: expression of galanin and receptors by progenitor cells in vivo and in vitro and effects of galanin on neurosphere proliferation. Neuropeptides 2005;39:201–205.

7 Lündstrom L, Elmquist A, Bartfai T, Langel Ü: Galanin and its receptors in neurological disorders. Neuromol Med 2005;7:157–180.

8 Hobson SA, Bacon A, Elliot-Hunt CR, Holmes FE, Kerr NCH, Pope R, et al: Galanin acts as a trophic factor to the central and peripheral nervous systems. Cell Mol Life Sci 2008;65:1806–1812.

9 Zumkeller W: The effect of insulin-like growth factors on brain myelination and their potential therapeutic application in myelination disorders. Eur J Paediatr Neurol 1997;4:91–101.
10 Kühl NM, Hoekstra D, De Vries H, De Keyser J: Insulin-like growth factor-binding protein 6 inhibits survival and differentiation of rat oligodendrocyte precursor cells. Glia 2003;44:91–101.
11 Jin K, LaFevre-Bernt M, Sun Y, Chen S, Gafni J, Crippen D, et al: FGF-2 promotes neurogenesis and neuroprotection and prolongs survival in a transgenic mouse model of Huntington's disease. Proc Natl Acad Sci USA 2005;102:18189–18194.
12 Molteni R, Fumagalli F, Magnaghi V, Roceri M, Gennarelli M, Racagni G, et al: Modulation of fibroblast growth factor-2 by stress and corticosteroids: from development events to adult brain plasticity. Brain Res Rev 2001;37:249–258.
13 Bansal R, Magge S, Winkler S: Specific inhibitor of FGF receptor signaling: FGF-2-mediated effects on proliferation, differentiation, and MAPK activation are inhibited by PD173074 in oligodendrocyte-lineage cells. J Neurosci Res 2003;74:486–493.
14 Drake AJ, Walker BR, Seckl JR: Intergenerational consequences of fetal programming by in utero exposure to glucocorticoids in rats. Am J Physiol 2005;288:R34–R38.
15 Seckl JR, Cleasby M, Nyirenda MJ: Glucocorticoids, 11β-hydroxysteroid dehydrogenase, and fetal programming. Kidney Int 2000;57:1412–1417.
16 Felig P, Frohman LA: Endocrinology and Metabolism. New York, McGraw-Hill, 2001.
17 Doan T, Melvold R, Viselli S, Waltenbaugh C: Lippincott's Illustrated Reviews: Immunology. Philadelphia, Lippincott Williams & Wilkins, 1997.
18 Neugebauer R, Hoek HW, Susser E: Prenatal exposure to wartime famine and development of antisocial personality disorder in early adulthood. JAMA 1999;281:455–462.
19 Baum DA, Smith SD, Donovan SS: The tree-thinking challenge. Science 2005;310:979–980.
20 Sharif J, Nakamura M, Ito T, Kimura Y, Nagamune T, Mitsuya K, et al: Food restriction in pregnant mice can induce changes in histone modifications and suppress gene expression in fetus. Nucleic acids Symp Ser (Oxf) 2007;51:125–126.
21 Matsuda N, Velayo C, Ito T, Chisaka H, Yaegashi N, Kimura Y, Okamura K, Sharif J: Gestational stage- and sex-specific impact of maternal folate deficiency on fetal growth and epigenetic regulation of gene expression in the fetus. Reprod Sci Suppl 2009;16:140A–141A.
22 Velayo C, Matsuda N, Ito T, Chisaka H, Yaegashi N, Kimura Y, Okamura K, Sharif J: Maternal protein restriction during late gestation induces sex-specific and reciprocal regulation of the Igf2/Igfbp1 gene expression ratio in placenta: a possible association between nutrition and epigenetics. Reprod Sci Suppl 2009;16:347A–347A.
23 Meijer MK, Spruijt BM, van Zutphen LFM, Baumans V: Effect of restraint and injection methods on heart rate and body temperature in mice. Lab Anim 2006;40:382–391.
24 Ryabinin AE, Wang YM, Finn DA: Different levels of Fos immunoreactivity after repeated handling and injection stress in two inbred strains of mice. Pharm Biochem Behav 1999;63:143–151.

Med Biol Eng Comput (2009) 47:1075–1082
DOI 10.1007/s11517-009-0528-y

ORIGINAL ARTICLE

Antepartum non-invasive evaluation of opening and closing timings of the cardiac valves in fetal cardiac cycle

Ahsan H. Khandoker · Yoshitaka Kimura · Takuya Ito · Naoaki Sato · Kunihiro Okamura · Marimuthu Palaniswami

Received: 14 January 2009 / Accepted: 17 August 2009 / Published online: 27 August 2009

Abstract In this study, we propose a non-invasive algorithm to recognize the timings of fetal cardiac events on the basis of analysis of fetal ECG (FECG) and Doppler ultrasound signals. Multiresolution wavelet analysis enabled the frequency contents of the Doppler signals to be linked to the opening (o) and closing (c) of the heart's valves (Aortic (A) and Mitral (M)). M-mode, B-mode and pulsed Doppler ultrasound were used to verify the timings of opening and closure of these valves. In normal fetuses, the time intervals from Q-wave of QRS complex of FECG to opening and closing of aortic valve, i.e., Q-Ao and Q-Ac were found to be 79.3 ± 17.4 and 224.7 ± 13.3 ms, respectively. For the mitral valve, Q-Mc and Q-Mo were found to be 27.7 ± 9.4 and 294.6 ± 21.3 ms, respectively. Correlations among the timings in opening and closing of cardiac valves were found to be higher in abnormal fetuses than that in normal ones.

A. H. Khandoker (✉) · M. Palaniswami
Department of Electrical and Electronic Engineering, The University of Melbourne, Parkville, Melbourne, VIC 3010, Australia
e-mail: ahsank@unimelb.edu.au

Y. Kimura · T. Ito
Institute of International Advanced Interdisciplinary Research, Tohoku University School of Medicine, Seiryo-cho, Sendai 980-8575, Japan

N. Sato
Department of Gynecology and Obstetrics, Tohoku University Hospital, Seiryo-cho, Sendai 980-8575, Japan

K. Okamura
Graduate School of Medicine, Tohoku University School of Medicine, Seiryo-cho, Sendai 980-8575, Japan

Keywords Fetal electrocardiogram · Doppler ultrasound · Wavelet · Fetal cardiac function · Fetal monitoring

1 Introduction

Fetal ECG and Doppler ultrasound (DUS) signals provide clinically significant information about the physiological state of a fetus. The evaluation of fetal cardiac activity has received limited attention. It is known that congenital heart defects (CHD) and fetal distress (e.g., low oxygen levels in fetus) are the most common major causes of congenital abnormalities and fetal mortality. The prevalence of CHD is 3–8 per 1,000 pregnancies at birth [1]. Studies have shown that an early detection of some fetuses with potentially ductal-dependent CHD results in an improvement of hemodynamic status, neonatal morbidity, and surgical outcome [2]. Fetal distress is associated with postmaturity (when the placenta malfunctions in a post-term pregnancy), or with complications of pregnancy, or labor that affects the mother and therefore also affect their fetus. The determination of CHD and fetal distress during fetal life, where the examiner must deal with a patient who cannot be visualized directly and is located within another individual, presents unique challenges.

Structural defects cause abnormal heart rhythm such as long QT (LQT) syndrome. LQT syndrome is characterized by the presence of a prolonged QT interval on electrocardiography (ECG) and a high risk for developing life-threatening arrhythmias and sudden cardiac death in children and adults [3]. There have been two reports describing prenatal cardiotocographic findings in fetuses with LQT syndrome [4, 5]. However, to our knowledge, definitive prenatal diagnosis of this congenital syndrome has not been described.

Maternal risk factors and a large number of intrapartum causes lead to fetal hypoxia. Diagnostics of a distressed unborn baby are mainly aimed at detection of occurrence of intrauterine hypoxia. Consequences resulting from fetal hypoxia appear in its heart activity [6]. In perinatal medicine, non-invasive cardiotocography (CTG), which is a record of the fetal heart rate (FHR) and uterine contraction activity measured via transducer on the abdomen, is commonly used. Sometimes abnormal variability in FHR may not necessarily represent the fetus in distress.

The systolic time intervals (STI) of the fetal cardiac cycle have been analyzed by several authors in the past. The pre-ejection period (PEP) and left ventricular ejection time (VET) are reported to be sensitive markers of fetal cardiac performance [7]. PEP, which is defined as the interval between the onset of the QRS complex of fetal ECG and the start of ventricular ejection (i.e., the opening of aortic valve), is known to be a sensitive indicator of myocardial performance [8]. VET is the time interval from opening to closure of semilunar or aortic valve, during which blood is flowing from ventricle into outflow. In clinical studies, prolongation of PEP during antepartum period was associated with a high incidence of perinatal abnormalities [7]. There is a method that uses systolic time interval (STI) which can be calculated with an invasively measured fetal electrocardiogram (FECG) via scalp electrodes and a Doppler shift of ultrasound beam reflected from moving valves of the fetal heart. Even though it can provide high diagnostic sensitivity, that method cannot be applied until the rupture of membranes. Notwithstanding the importance of monitoring fetal cardiac performance with the systolic time intervals, the reasons why it has not been widely applied in clinical practice include the difficulty in obtaining a reliable simultaneous recording of fetal ECG and DUS signals. A new research paradigm is, therefore, required to address this problem. In this study, for better diagnosing fetus prenatally, we propose a novel non-invasive algorithm to recognize the timings of fetal cardiac events on the basis of electrical (fetal ECG extracted from abdominal ECG) and mechanical (DUS signals) heart activity. We verify the timings of opening and closing of aortic and mitral valves with simultaneously recorded pulsed Doppler images.

2 Methods

Simultaneous recording of the abdominal ECG signals and DUS signals from 21 pregnant women at the gestational age of 28–36 weeks with normal single pregnancies and eight pregnant women who were diagnosed to have fetal abnormalities (heart anomaly (5), LQT syndrome with heart anomaly (2), acute hypoxia for early separation of placenta (1)) were collected from Tohoku University Hospital. A total of 29 recordings (each of 1 min length) were sampled at 1,000 Hz with 16-bit resolution. The study protocol was approved by Tohoku University Institutional Review Board and written informed consent was obtained from all subjects.

The continuous DUS data were obtained using Ultrasonic Transducer 5700 (fetal monitor 116, Corometrics Medical Systems Inc.) with 1.15 MHz signals. To compare the actual appearance of the aortic valve's opening and closing pattern with valve timing events appeared in DUS signals, M-mode, B-mode, and pulsed-wave Doppler signals were obtained from convex 3.5 Hz of HITACHI ultrasound scanner (Ultrasonic diagnostic instrument Model EUB-525; HITACHI health medical corporation). The detailed procedure for experimental set up and transabdominal ECG data collection has been described in our previous study [9]. FECG traces were extracted using a method that combines cancellation of the mother's ECG signal and the blind source separation with reference (BSSR) as described in our earlier study [9]. Briefly, the cancellation of the mother's ECG component was performed by subtracting the linear combination of mutually orthogonal projections of the heart vector. After removing maternal ECG, BSSR, which is a kind of neural network methods, extracted fetal ECG signals from complex mixed signals using DUS signal as reference signal [9].

2.1 Timings of valve motions in fetal cardiac cycle

Timings of fetal cardiac valve motions and wall movements have been illustrated in the study of the fetal heart's physiology [7]. Atrial contraction is initiated by the P wave while ventricular contraction is related to R wave activity, hence significant content in the ultrasound signal may be expected at these times. Since both sides of the heart are in synchrony and due to the simultaneous operation of the pulmonic & aortic (semilunar) valves and the tricuspid & mitral (atrioventricular) valves, their individual activity cannot be expected to appear itself in the ultrasound signal [7, 10]. Figure 1 shows the relative opening and closing timings of the heart's aortic and mitral valves in relation to the FECG. Doppler frequency shifts associated with cardiac activity can be visualized. The PEP represents the entire interval from the onset of electrical excitation to aortic (semilunar) valve's opening. On the other hand, VET is the remaining systolic interval which is the interval from aortic valve opening to closure during which blood is flowing out from the ventricle into the aorta. DUS signals vary in time due primarily to variations in the relative orientation of the fetal heart and the ultrasound transducer [7]. Therefore, all timings of events of cardiac valves are unlikely to be distinguished in each cardiac cycle. Obviously, fetal movement greatly affects the received signal.

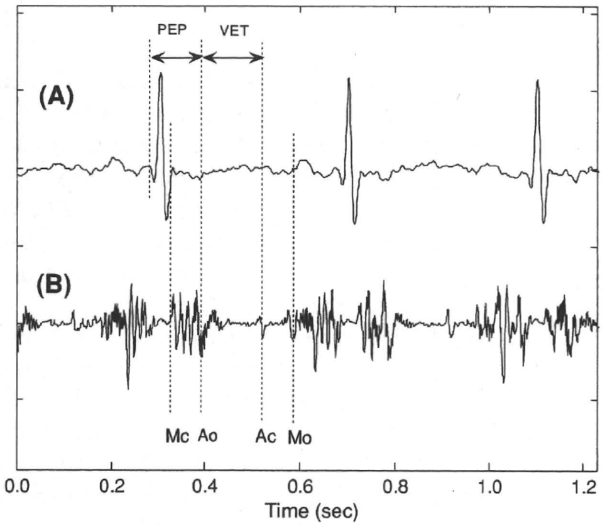

Fig. 1 Example of simultaneously recorded fetal ECG and Doppler ultrasound (DUS) data.(*A*) fetal ECG signal extracted from maternal abdominal signals using Blind source separation with reference (BSSR) [9]. (*B*) Data from the non-directional channel of the ultrasound from fetal heart. Annotations showing the timings of the opening and closing of the heart's aortic and mitral valves in relation to the electrocardiogram. Aortic (A), Mitral (M), opening (o), closing (c). *PEP* pre-ejection period, *VET* left ventricular ejection time

2.2 Wavelet analysis of DUS signals

Interpretation of DUS signals in relation to cardiac valve movements was performed using time frequency wavelet analysis. Wavelet analysis has become a powerful tool for analysis of non-stationary signals whose spectral characteristics change significantly over time. A wavelet transform (WT) uses a set of basis functions to decompose a signal into the detailed signals and the approximate signals of the original signal. The complex Gaussian with order 2 was used as mother wavelet in this study. To extract the higher frequency content, the detailed component of the DUS signal at level 2 (100–200 Hz) was processed. The maxima of the absolute value of the detailed signals were fitted by an envelope of cubic splines.

3 Results

The use of M-mode, B-mode, and pulsed DUS to examine the opening and closing timings of the aortic valve is shown in Fig. 2. M-mode is a useful adjunct to the fetal cardiovascular examination because it enables the

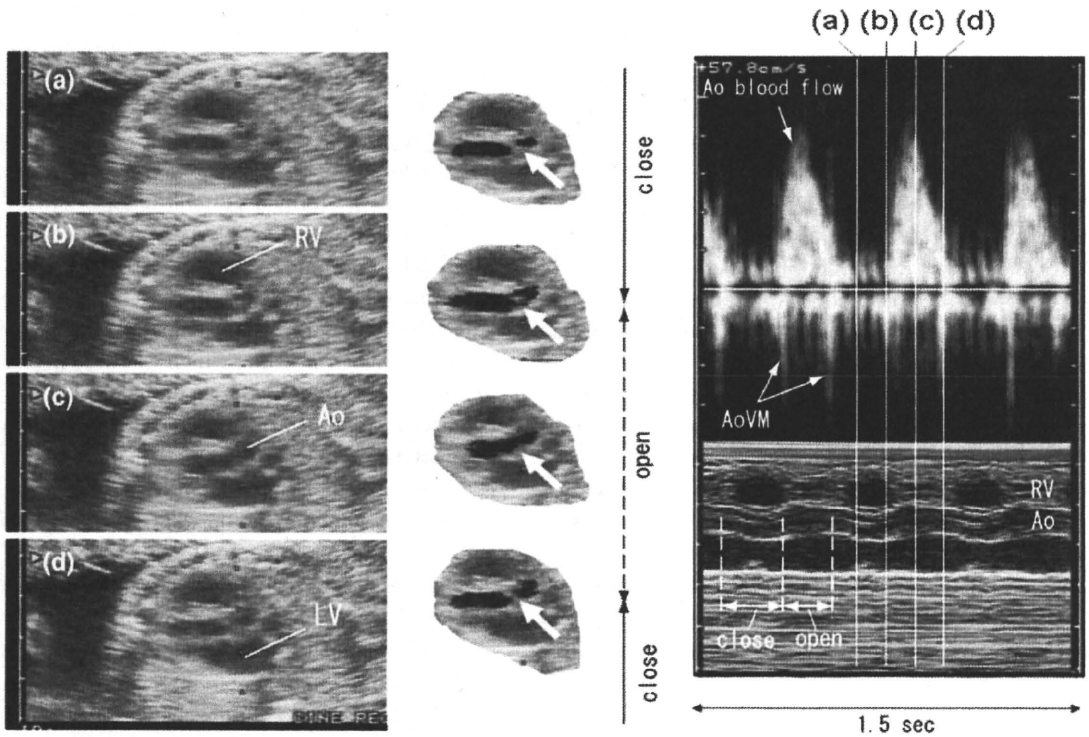

Fig. 2 *Left panels* show B-mode views of a fetal aortic valve movements. The *middle panels* are the images extracted from B-mode views. *White arrows* show the aortic valve. *Panel* (*a*) shows the closing of the aortic valve, (*b*) shows the start of opening of the aortic valve, (*c*) shows that aortic valve is open and (*d*) shows that aortic valve is closed. The *right panels* show the pulsed-wave Doppler signals during the opening and closing time of the aortic valve and its M-mode image at the same time phases. *RV* right ventricle, *Ao* aorta, *LV* left ventricle, and *AoVM* aortic valve movement

physician to obtain the exact measurement of valve's structure. Pulsed Doppler examination demonstrates the direction and the characteristics of blood flow within the heart. The aortic blood flow Doppler waveform was recorded from the long axis of the five-chamber view of the heart. The M-mode cursor was placed perpendicular to the inter-ventricular septum at the level of the mitral valve to examine end-systole and end-diastole (closure of atrio-ventricular valves).

Two examples of the FECG for several cardiac cycles together with DUS signals and their detailed signals at level 2 wavelet decomposition are shown in Figs. 3 and 4. The timings of aortic valve motions (in Fig. 3) and mitral valve motions (in Fig. 4) with respect to the ECG, the origin of the events highlighted within the DUS were elucidated and verified by pulsed DUS in the bottom panel. In order to detect the peak timings of aortic valve's motion events, the time durations from R wave within each RR interval chosen for detecting each event were 0.05–0.10 s for Ao and 0.14–0.26 s for Ac. On the other hand, for mitral valve's relative timings, 0.00–0.05 s for Mc and 0.26–0.33 s for Mo were used in calculation. Although the QT interval can be obtained following delivery using ECG, this is not feasible in utero. The electromechanical Q-Ac interval which is measured from the onset of Q-wave to aortic valve closing, represent QT intervals which can be corrected for heart rate.

Table 1 shows analysis results presented as the mean duration of the aortic valve's opening and closing events from the onset of Q-wave of FECG namely Q-Ao and Q-Ac within each RR interval.

There were cases where all events could easily be recognized. However, there were also cases where only particular events were observed. Number and rates of successfully identified events have been summarized in Table 1. No significant differences were found among the valve timing intervals of the two groups.

Tables 2 and 3 summarize the correlations among the valve opening and closing timings. Significant correlations were found among valve timings in abnormal fetuses as compared to that in normal fetuses. Q-Ao i.e., PEP was found to be strongly correlated ($r = 0.496$, $P = 0.0013$) with R-R intervals in abnormal fetuses. On the other hand, very weak correlation ($r = 0.0448$, $P = 0.459$) was found in normal fetuses. Correlation between R-R and Q-Mc was found to be positive for normal fetuses, however, negative for abnormal fetuses. Similarly, Q-Mc and Q-Ac were found to be positively and negatively correlated in abnormal and normal fetuses respectively. Correlation between Ac-Ao (i.e., VET) and R-R intervals was found to be significantly higher in normal fetuses than in abnormal fetuses.

4 Discussion

Fetal ECG and DUS signals provide clinically significant information concerning the physiological state of a fetus. This study provided a simple and noninvasive technique to simultaneously record and estimate fetal cardiac valve (aortic and mitral) timings with reference fetal ECG. This method has advantages over M-mode and pulsed Doppler in its simplicity and accuracy in the measurement of electromechanical time intervals.

The systolic time intervals of the fetal cardiac cycle have been analyzed by several authors in the past by using pulsed Doppler and M-mode echocardiography [11], digital filtering of DUS [7, 8, 12, 13], frequency spectrogram of DUS by short term fourier transform (STFT) [10]. Shakespeare [10] applied short-time Fourier transform to DUS signals from fetal heart and carried out identification of fetal heart events such as valve and wall motions observed in Doppler signal as well as determination of relations between them. Kupka [14] showed high correlation (Ao:0.92, Ac:0.87, Mo:0.87, Mc:0.63) between spectrums of events of same type from two consecutive cycles. They suggested that the time frequency analysis of fetal Doppler signal should be able to distinguish fetal heart events and improve the current performance of DUS-based FHR monitors. Although the appearance of particular type of events in fetal heart motion strongly depends on location of ultrasound transducer, our algorithm can continuously measure the fetal heart events by placing ultrasound transducers. The acoustic heartbeats from loudspeaker were previously used to achieve a proper determination of FHR signals performed by fetal monitor [14]. Analysis of FHR variability has recently been used to identify growth-restricted compromised fetus [15, 16]; however, parameter selection of HRV analysis may potentially compromise the applicability of those analysis techniques in general.

The wavelet transform, which was used in this study, was developed as an alternative approach to the STFT to overcome the resolution problem. The wavelet analysis is done in a similar way to the STFT analysis, in the sense that the signal is multiplied with a function, the mother wavelet, similar to the window function in the STFT, and the transform is computed separately for different segments of the time-domain signal. The STFT gives a fixed resolution at all times, whereas the WT gives a variable resolution. The width of the window is changed as the transform is computed for every single spectral component, which is probably the most significant characteristic of the wavelet transform.

Identification of movements of cardiac valves would have been very difficult without the FECG. In this study, the position of the R wave helps detect the timing of fetal cardiac valve movements.

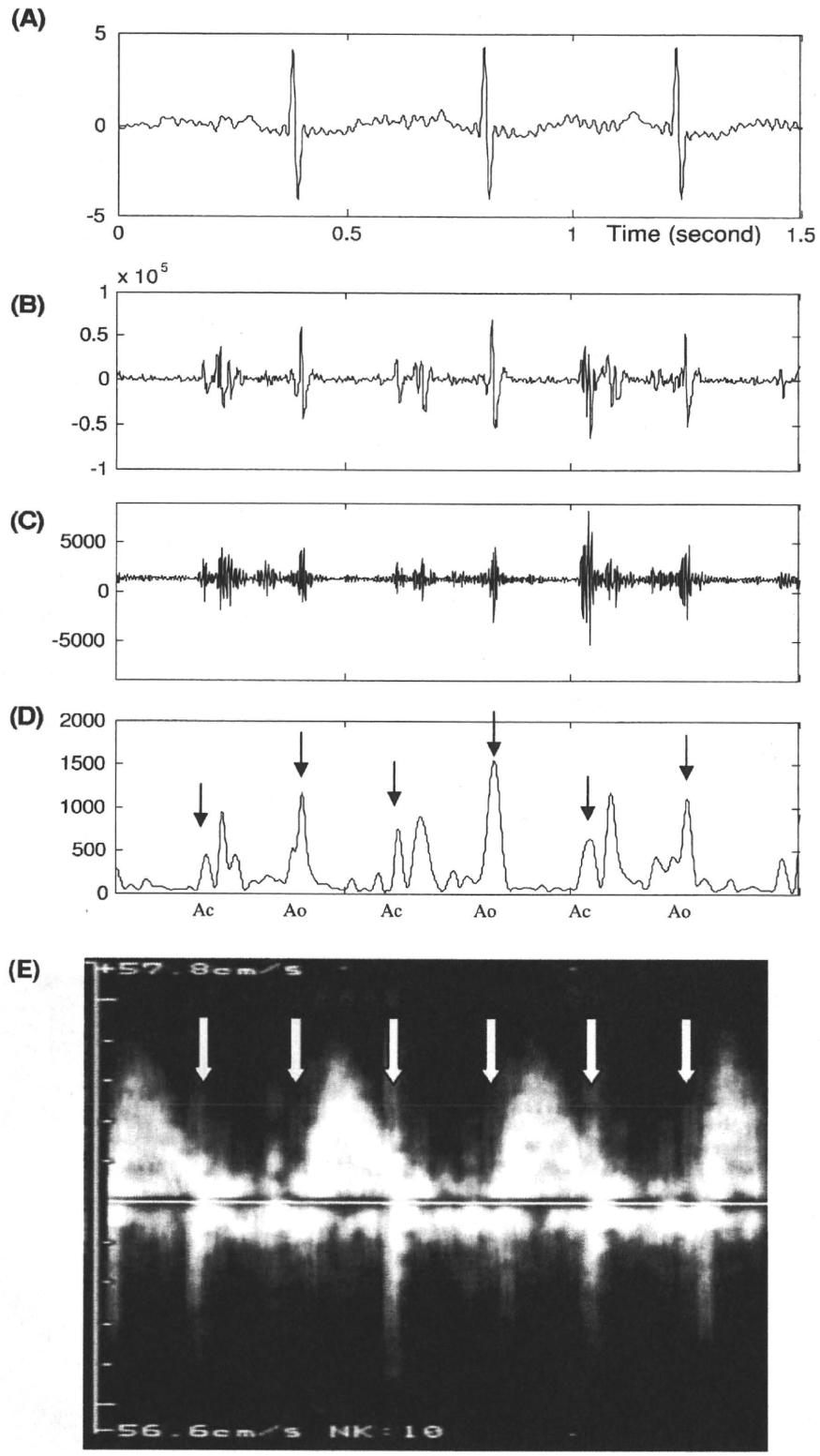

Fig. 3 **a** Shows an example of fetal electrocardiogram signals extracted from abdominal ECG signals using BSSR [9]. **b** Shows the simultaneous Doppler ultrasound signals from fetal monitor 116. **c** Shows the detailed signal after wavelet decomposition of **b** at level 2. **d** Shows the cubic splines envelope of maxima of the detailed signal in panel **d**. **e** Shows the example of Pulsed-wave Doppler signals of fetal aortic valve movements annotated to show how the specific signals are linked with opening and closing events. Ao and Ac represent the opening and closing of aortic valve

In normal healthy fetuses, PEP duration was reported not to be influenced by heart rate variation, but VET (i.e., Ac-Ao) was reported to be inversely correlated with heart rate [7]. Our findings support that claim. The correlations of valve timing intervals in abnormal fetuses were found to be significant. We speculate that the control

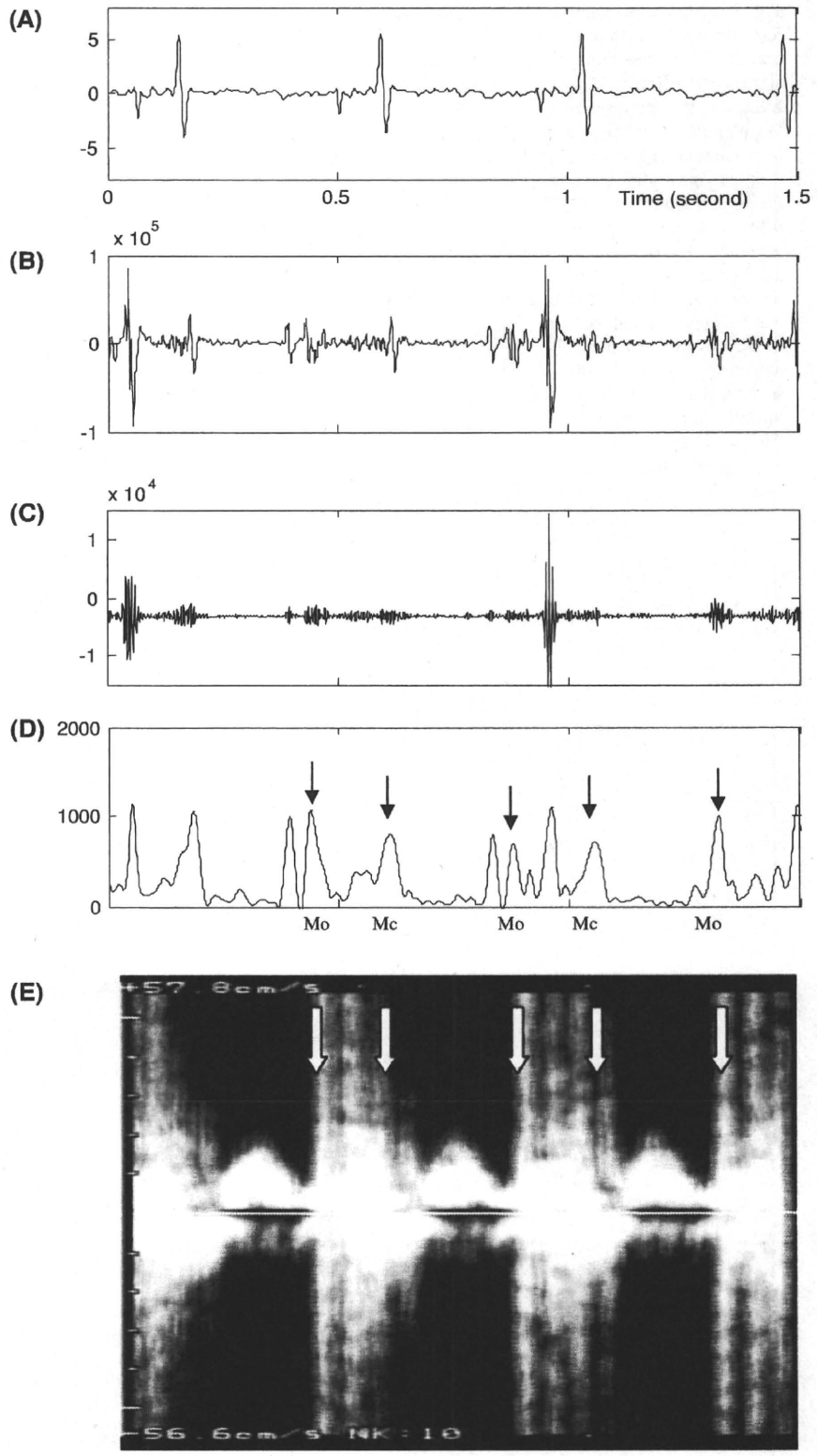

Fig. 4 **a** Shows an example of fetal electrocardiogram signals extracted from abdominal ECG signals using BSSR [9]. **b** Shows the simultaneous Doppler ultrasound signals from fetal monitor 116. **c** Shows the detailed signal after wavelet decomposition of **b** at level 2. **d** Shows the cubic spline envelope of maxima of the detailed signal in panel **d**. **e** Shows the example of Pulsed-wave Doppler signals of fetal mitral valve movements annotated to show how the specific signals are linked with opening and closing events. Mo and Mc represent the opening and closing of mitral valve

mechanism for heart contraction in abnormal fetuses is different from that in healthy fetuses that could relate to the rigidity of the fetal heart contraction control system in abnormal fetuses. Less flexibility in cardiac valves' opening and closing in the abnormal fetuses may have contributed to significantly correlated valve movement and

Table 1 Summary (mean ± SD) of time intervals (ms) of opening and closing of the aortic and mitral valves from FECG and Doppler ultrasound signals over a cardiac cycle (number of successfully identified events and rates %)

	R-R	Q-Mc	Q-Ao	Q-Ac	Q-Mo	Ac-Ao
Normal fetuses (21)	421 ± 33 (2263)	27.7 ± 9.4 (1910; 84.4%)	79.3 ± 17.4 (1970; 87.0%)	224.7 ± 13.3 (2210; 97.6%)	294.6 ± 21.3 (2030; 89.70%)	144 ± 26.7 (1970; 87.0%)
Abnormal fetuses (8)	433 ± 20 (889)	29.5 ± 4.4 (810; 91.1%)	81 ± 22.4 (830; 93.3%)	228.5 ± 15.9 (885; 99.5%)	289.0 ± 23.8 (870; 97.8%)	147 ± 10.2 (830; 93.3%)

Table 2 Correlations (r) among fetal heart rate and cardiac valve's timing intervals for the normal fetuses

	R-R	Q-Mc	Q-Ao	Q-Ac	Q-Mo	Ac-Ao
R-R	1	−0.077	0.044	0.445*	0.429*	0.680*
Q-Mc		1	0.066	−0.077	0.123	0.061
Q-Ao			1	−0.124	0.038	0.809*
Q-Ac				1	0.287*	0.665*
Q-Mo					1	0.083
Ac-Ao						1

*Significance at $P < 0.01$

Table 3 Correlations (r) among fetal heart rate and cardiac valve's timing intervals for the abnormal fetuses

	R-R	Q-Mc	Q-Ao	Q-Ac	Q-Mo	Ac-Ao
R-R	1	0.460*	0.496*	0.441*	0.845*	0.066
Q-Mc		1	−0.032	0.483*	0.517*	0.091
Q-Ao			1	0.014	0.658*	0.073
Q-Ac				1	0.421*	0.185
Q-Mo					1	0.676*
Ac-Ao						1

*Significance at $P < 0.01$

timing intervals. In eight abnormal fetuses, six heart anomaly cases had tetralogy of Fallot and double outlet right ventricle, while two LQT syndromes with heart anomaly had single ventricle and dilatation of heart. Dysfunction of the control system in heart anomaly or acute emergency state of fetus could be considered factors behind the differences in correlation parameters. But the precise explanation requires further research which will be attempted in the future study.

Multiresolution wavelet analysis enabled the frequency contents of the Doppler signals to be linked to the opening and closing of the aortic and mitral valves as confirmed by M-mode and pulsed Doppler images. These results suggest means by which the cardiac events that contribute to the Doppler signal may be distinguished, providing potential clinical application for better recognition of fetal compromise and distress such as fetal arrhythmia, anoxia, and heart failure. Results of this study could make it possible to record PEP and VET of fetal heart continuously in real time. Further research on modeling of the relationship of timings of cardiac valves (aortic as well as mitral) with R-R intervals over a wider range will be attempted on a diverse sample size.

Acknowledgements This study was supported by an Early career researcher (ECR) grant awarded to AH Khandoker by University of Melbourne with partial support received from Australian Research Council (ARC) research networks on Intelligent sensing, sensor networks and information processing (ISSNIP). The authors would like to thank Dr Slaven Marusic and Dr Mak Daulatzai of University of Melbourne for revising and editing the manuscript.

References

1. Ferencz C, Rubin JD, McCarter RJ (1985) Congenital heart disease: prevalence at live birth. The Baltimore-Washington infant study. Am J Epidemiol 121:31–36
2. Bonnet D, Coltri A, Butera G et al (1999) Detection of transposition of the great arteries in fetuses reduces neonatal morbidity and mortality. Circulation 99:916–918
3. Schwartz PJ (1997) The long QT syndrome. Curr Probl Cardiol 22:297–351
4. Vigliani M (1995) Romano-Ward syndrome diagnosed as moderate fetal bradycardia: a case report. J Reprod Med 40:725–728
5. Hofbeck M, Ulmer H, Beinder E, Sieber E, Singer H (1997) Prenatal findings in patients with prolonged QT interval in the neonatal period. Heart 77:198–204
6. Matonia A, Jezewski J, Kupka T, Wrobel J, Horoba K, Widera M (2005) Instrumentation for fetal cardiac performance analysis during the antepartum period. In: Proceedings of the IEEE engineering in medicine and biology 27th annual conference, NY, pp 1–4
7. Murata Y, Martin CB (1974) Systolic time intervals of the fetal cardiac cycle. Obstet Gynecol 44:224–232
8. Goodlin RC, Girard J, Hollmen A (1968) Systolic time intervals in the fetus and neonate. Circulation 37:149–159
9. Sato M, Kimura Y, Chida S, Ito T, Katayama N, Okamura K, Nakao M (2007) A novel extraction method of fetal electrocardiogram from the composite abdominal signal. IEEE Trans Biomed Eng 54(1):49–58
10. Shakespeare SA, Crowe JA, Hayes-Gill BR, Bhogal K, James DK (2001) The information content of Doppler ultrasound signals from the fetal heart. Med Biol Eng Comput 39:619–626
11. Tsyvian P, Malkin K, Wladimiroff JW (1995) Assessment of fetal left cardiac isovolumic relaxation time in appropriate and small-for-gestational-age-fetuses. Ultrasound Med Biol 21:739–743
12. Hawrylyshyn PA, Benstein A, Organ LW (1982) Fetal preejection period. Obstet Gynecol 59:747–754
13. Koga T, Athayde B, Trundinger B, Nakano H (2001) A new and simple Doppler method for measurement of fetal cardiac isovolumetric contraction time. Ultrasound Obstet Gynecol 18:264–267
14. Kupka T, Jezewski J, Matonia A, Horoba K, Wrobel J (2004) Timing events in Doppler ultrasound of fetal heart activity. In:

Proceedings of the 26th annual international conference of the IEEE EMBS San Francisco, CA, USA September 1–5, 2004
15. Ferrario M, Signorini MG, Magenes G (2009) Complexity analysis of the fetal heart rate variability: early identification of severe intrauterine growth-restricted fetuses. Med Biol Eng Comput. doi:10.1007/s11517-009-0502-8
16. Gonçalves H, Rocha AP, Ayres-de-Campos D, Bernardes J (2006) Linear and nonlinear fetal heart rate analysis of normal and acidemic fetuses in the minutes preceding delivery. Med Biol Eng Comput 44(10):847–855

社団法人 電子情報通信学会
THE INSTITUTE OF ELECTRONICS,
INFORMATION AND COMMUNICATION ENGINEERS

信学技報
IEICE Technical Report

1 計測信号参照系独立成分分析法のシミュレーション研究

幡谷速昭[1] 木村芳孝[2] 伊藤拓哉[2] 辛島彰洋[1] 片山統裕[1] 八重樫伸生[2] 中尾光之[1]

1 東北大学大学院情報科学研究科, 〒980-8579 宮城県仙台市青葉区荒巻字青葉 6-3-09

2 東北大学先端医工研究機構, 〒980-8575 宮城県仙台市青葉区星陵町 2-1

E-mail: hataya@biomdl.ecei.tohoku.ac.jp

あらまし 1計測信号から複数の独立成分を分離抽出する single-ICA はその有用性が期待される一方，分離精度にまだ問題があり改良の余地が多く残されている．我々は参照系独立成分分析法を用いた簡便な single-ICA のアルゴリズムを新たに提案し，多次元の埋め込み行列を作成する際の次元数と間引き間隔の変化に対する分離結果を調べた．その結果，分離信号の精度と原信号との時間のずれの変化の仕方は，各分離信号で異なることがわかった．この変化の仕方の違いが信号のどのような性質によるものであるか考察し，求めたい信号に応じた次元数と間引き幅の適切な設定に役立てたい．

キーワード single ICA, blind source separation with references (BSSR), 胎児心音，雑音除去

A Simulation Study of Single-BSS with References

Toshiaki HATAYA[1] Yoshitaka KIMURA[2] Takuya ITO[2] Akihiro KARASHIMA[1]

Norihiro KATAYAMA[1] Nobuo YAEGASHI[2] and Mitsuyuki NAKAO[1]

1 Graduate School of Information Sciences, Tohoku University, 6-3-09, Aramaki-aza-aoba, Aoba-ku, Sendai, Miyagi, 980-8579, Japan

2 Tohoku University Biomedical Engineering Research Organization, 2-1, seiryou-chou, Aoba-ku, Sendai, Miyagi, 980-8575, Japan

E-mail: :hataya@biomdl.ecei.tohoku.ac.jp

Abstract Single-ICA can be very useful method to extract independent components from signal observed by single channel. But there is still a problem in the accuracy of separation and a lot to work on. We propose a simple single-ICA algorithm using blind source separation with references, and investigate the changes in the accuracy of separation and time gap between extracted signal and source signal, by altering the dimension and the lag time of the multi-dimensional embedded matrix. Then the result is that each extracted signal shows different change characteristics for the increase of dimension and lag time. Considering the property that causes these change characteristics, we are expecting these results to be helpful for optimal design of dimension and lag time.

Keyword single-ICA, blind source separation with reference (BSSR), fetal heart sound (FHS), denoising

1. はじめに

1計測信号からの複数独立信号の分離抽出については様々な研究がなされてきた．一例として，心音図からの胎児心音の分離を試みている論文[1]を挙げる．ここでは計測信号を多次元の埋め込み行列に拡張してICAを行った後に，得られた信号を周波数成分の違いに基づいてクラスタリングして複数の独立成分を得る手法を用いている．結果として分離はうまくいっているように見えるが，時間の基準を与えずにICAを行うので時間方向の混合が起こるといった問題がある．また，彼らは埋め込み行列の適切な設定について言及しているが，それらの値の変化によって分離信号がどのように変化するかについては述べられていない．

本研究では参照系独立成分分析[2]を用いた新しいsingle-ICAでシミュレーションを行い，埋め込み行列の次元数と間引き間隔の変化による，分離信号の精度の変化について調べた．最後にその結果を基に，適切な次元数と間引き間隔の設定について検討したので報告する．

2. 1計測信号参照系独立成分分析

1次元の計測信号を $\mathbf{x}=(x_1,x_2,...,x_n)$ とする．ICAを用いて複数の信号を得るためには，この計測信号を